High-Speed Traveling-Wave Modulator based on Graphene and Microfiber

Ke Xu, *Member, IEEE,* Yongqiang Xie, Hucheng Xie, Yingjie Liu, Yong Yao, Jiangbing Du, *Member, IEEE,* Zuyuan He, *Senior Member, IEEE,* and Qinghai Song

***Abstract*—The two-dimensional graphene has an extremely high carrier mobility which can potentially offer an electrical bandwidth of over 500 GHz. However, the bandwidth of the reported graphene-based modulators is only a few tens of gigahertz due to the limitation of RC constant rather than the carrier transit time. In this work, a high-speed traveling-wave electro-optic modulator based on graphene/microfiber structure is proposed and investigated for the first time to our best knowledge. The all-in-fiber electro-optic modulation in the graphene/microfiber-modulator is achieved by changing the Fermi level of graphene during its interaction with the evanescent wave of the microfiber. The active length of the modulator is 1.372 mm with a V_π of 4.9 V. The coplanar strip electrodes have a characteristic impedance of 54 ohm and a microwave attenuation of 0.967 dB/mm. The mismatch between the microwave and the optical group velocity is 7.38 %. A very high speed of 82 GHz 3-dB bandwidth is achieved.**

***Index Terms*—Modulator, graphene, traveling wave electrode.**

I. Introduction

Two-dimensional (2D), atom-thick materials have attracted a lot of interests in the research fields of both photonics and electronics during the past decade. With only a single layer of carbon atoms, graphene exhibits many amazing properties like zero band gap, linear dispersion, high Kerr nonlinearity, tunable Fermi level, large thermal-optic coefficient and remarkably high carrier mobility. These excellent optical and electrical properties make graphene a perfect candidate for a wide range of applications like broadband photodetection [1-3], nonlinear optics [4-6], saturable absorption [7-9], polarization handling [10], modulation [11] and so on. High-speed operation is a long-standing need in fiber optical communications and on-chip interconnects. The electrical bandwidth of the optoelectronic components has been scaled to a few tens of gigahertz [12, 13]. With an extremely high carrier mobility, graphene has a potential electrical bandwidth of ~ 500 GHz which is one order higher than the devices based on the current semiconductor technologies [11]. In addition to the superior electrical property, the layered graphene sheet is easy to integrate with optical fibers and photonic integrated circuits by mature deposition and transfer process. The aforementioned advantages make the integration of graphene and planar waveguides or optical fibers very attractive for many applications.

For optical fiber systems, external modulation is a preferred technique in terms of low chirp, high speed and capability for supporting advanced modulation formats, compared with the direct modulation of the laser. The commercial optical modulators however rely on integrated waveguides instead of silica fiber itself. The discrete packaged modulator has additional packaging cost and excess loss. Therefore, all-fiber modulator is highly desired for reducing the loss and simplifying the system to make the modulation better compatible with the fiber system. The modulators based on graphene/fiber graphene/silicon and graphene/silicon nitride have been widely demonstrated [14-23]. By now, the bandwidth of the demonstrated graphene-based modulators has not exceeded a few tens of GHz that is limited by the RC constant rather than the carrier transit time. Most of the demonstrated GFMs so far are based on lumped electrodes which require a very short device length to avoid the walk-off problem between optical and microwave signal. A thick enough gate dielectric is also needed to ensure a low capacitance. For both cases, the required driving voltage has to be increased. Besides, a systematic bandwidth analysis of the graphene-based modulators is yet to be reported.

In this paper, we propose an all-fiber traveling-wave graphene/fiber modulator (TWGFM) with a bandwidth of 82 GHz for the first time to our best knowledge. A systematic bandwidth investigation of the GFM has been carried out. The rest of the paper is organized as follows. Section II, the optical waveguide structure is designed. Section III, the traveling-wave electrode (TWE) is designed. The modulator's performance is evaluated, and the results are discussed. Section IV, the conclusions are given.

II. Optical Waveguide Design

The device structure of the TWGFM can be briefly depicted by Fig. 1 (a). Such a structure enables a top-gate voltage to be

This work is supported by the NSFC under grant 61505039, 61575051, 61675128, Shenzhen Fundamental research projects under the JCYJ20170307151047646, JCYJ20150529114045265 and Open Fund of IPOC 2016B005.

Y. Xie, H. Xie, Y. Liu, K. Xu, Y. Yao and Q. Song are with the Department of Electronic and Information Engineering, Harbin Institute of Technology (Shenzhen), Shenzhen 518055, China (E-mail: kxu@hit.edu.cn, yaoyong@hit.edu.cn, qinghai.song@hit.edu.cn).

J. Du and Z. He are with the State Key Laboratory of Advanced Optical Communication Systems and Networks, Shanghai Jiao Tong University, Shanghai 200240, China. (e-mail: dujiangbing@sjtu.edu.cn).

This article has been accepted for publication in a future issue of this journal, but has not been fully edited. Content may change prior to final publication. Citation information: DOI 10.1109/JLT.2018.2864606, Journal of Lightwave Technology

applied onto the device. The two layers of graphene almost fully cover the fiber which allows for the light-graphene

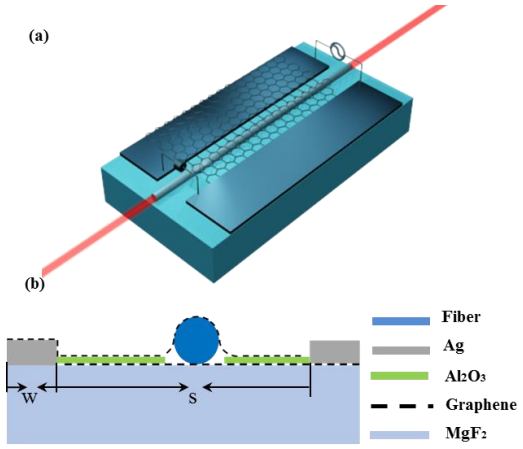

Fig. 1. (a) The schematic diagram of the proposed traveling wave electro-optic modulator structure. (b) The cross-section schematic of the device.

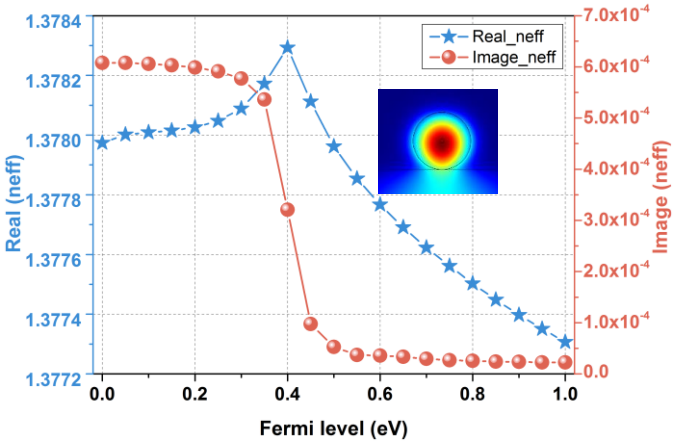

Fig. 2. The real (blue) and imaginary (red) part of complex effective mode index under different graphene's chemical potentials. Inset: The simulated optical field profile.

interaction as much as possible. The optical signal propagates in the microfiber and interacts with the graphene cladding. The microwave signal propagates along the TWE at a matched group velocity with the optical wave. The 50-ohm termination is applied at the end of the modulator. The schematic diagram of the device cross section is depicted in Fig.1 (b). The GFM is designed on the MgF_2 substrate which is transparent at infrared wavelengths. The refractive index of MgF_2 is a bit lower than the silica fiber which can reduce the amount of leakage into the substrate. The possible fabrication process of the TWGFM can be as follows. The bottom graphene layer is transferred onto the substrate and patterned. A thin layer of Al_2O_3 is then deposited as a gate dielectric. The electrodes are fabricated by another lift-off process, and the tapered microfiber is precisely placed onto the substrate afterwards. Finally, the top graphene layer is transferred and patterned by lithography.

The coplanar metal strips are designed as the traveling-wave electrodes which are 4.9 μm away from the microfiber. We have confirmed from simulations that this distance will induce negligible loss. The parameters of the electrode will be discussed in the electrode design part. In this section, we focus on the optical waveguide design first. The thickness of the top and bottom monolayer graphene is set to be 0.7 nm in the numerical model. The graphene's permittivity can be obtained from the optical conductivity which can be calculated by the

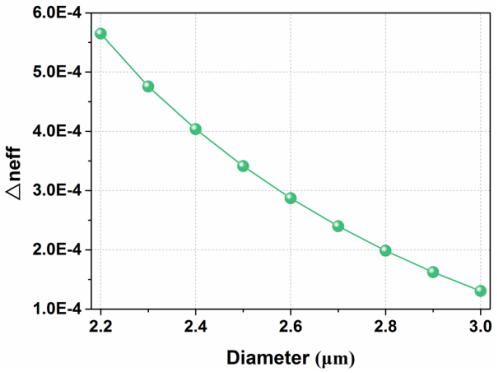

Fig. 3. The real part of effective mode index change under different microfiber diameters.

Kubo formula [24]. When the undoped graphene's Fermi level is higher than the half photon energy which is ~ 0.4 eV at 1550 nm wavelength, the light-graphene interaction is dominated by the intra-band absorption. The imaginary part of the graphene's complex permittivity becomes very small, and the graphene is nearly transparent. In contrast, the real part of the graphene's permittivity varies significantly under different Fermi levels which can be realized by applying a gate field onto the device. The optical mode field of the device cross section is shown as the inset of Fig. 2. Due to the small index difference between the fiber and the substrate, there is a small amount of leakage into the substrate. The calculated real part (blue) and imaginary part (red) of the optical mode effective indices under different graphene's Fermi levels are plotted in Fig. 2. Due to the graphene's unique property, the real part of the device n_{eff} varies significantly with the Fermi level above 0.5 eV. In this regime, the imaginary part of the n_{eff} is very small and does not change too much which allows for low absorption loss. As a result, a graphene/microfiber electro-optic modulator can be realized. The corresponding optical group refractive index is calculated to be 1.3788 at wavelength of 1550 nm when the Fermi level is 0.5 eV. The optical loss is calculated to be 9.5 dB/cm from the imaginary part of the complex index.

As an important parameter that determines the modulator efficiency, Δn is defined as the device effective index change when the graphene Fermi level varied from 0.5 eV to 9 eV. The effective index changes rely on the light graphene interaction, and thus is dependent on the amount of evanescent wave. The index changes are plotted under different fiber diameters as shown in Fig. 3. When the fiber diameter decreases, the interaction between the evanescent field and the graphene becomes more pronounced which results in a larger Δn. We set the fiber diameter to be 2.2 μm which results in a large Δn of ~5.65×10^{-4} when the Fermi level is tuned from 0.5 eV to 0.9 eV, as shown in Fig 3. It should be noted that the modulation efficiency is quite sensitive to the fiber diameter variation. This effect can be mitigated if the fiber is tapered slowly, and the device active length is not too long. The taper fiber with a diameter of 2.2 μm can be easily fabricated using the flame brushing technique [25]. It is possible to further reduce the diameter, but it increases the loss and the probability of fiber breaking as well. The real part of effective index change, Δn_{eff}

This article has been accepted for publication in a future issue of this journal, but has not been fully edited. Content may change prior to final publication. Citation information: DOI 10.1109/JLT.2018.2864606, Journal of Lightwave Technology

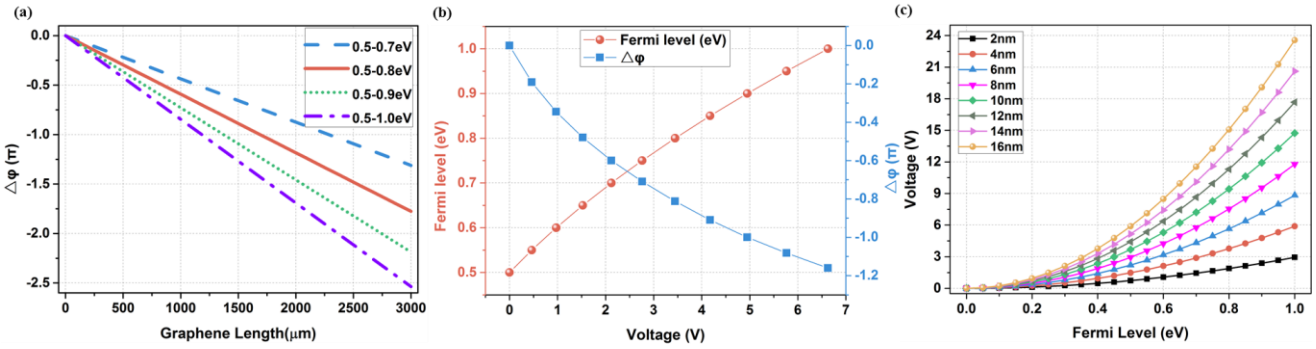

Fig. 4. (a) The phase changes under different Fermi levels ranges. (b) When the initial Fermi level is 0.5 eV, the Fermi level and the corresponding phase changes are calculated as a function of the applied voltage. (c) The relations between the voltage and Fermi level under different dielectric thickness.

give rise to a phase change which is described by

$$\Delta\varphi = \Delta n_{eff} L 2\pi/\lambda \quad (1)$$

where L represents the modulation length. Here we consider the graphene with an initial Fermi level of 0.5 eV and then calculate the phase changes when the Fermi level is increased. The phase change as a function of the device length L under different Fermi level tuning ranges is shown in Fig. 4 (a). Let us consider the Fermi level tuned from 0.5 eV to 0.9 eV shown as the green dot curve. The corresponding Δn is ~5.65×10^{-4}, the L_π is 1.372 mm, and the optical loss is 1.6 dB. To reduce the required gate voltage for Fermi level tuning, we can further increase the device length L. The relationship between the Fermi level change and the required driving voltage can be calculated using the method described in [26]. The Fermi level and the phase change as a function of the driving voltage is plotted in Fig. 4 (b). It can be seen that the V_π is ~ 4.9 V. As mentioned before, the V_π can be further reduced by using longer active length. Here we have to emphasize that the modulation efficiency is highly dependent on the dielectric thickness. We have shown the conversion between the Fermi level and the driving voltage under different dielectric thickness in Fig. 4 (c). To reduce the power consumption, the dielectric layer should be thin enough. For the lumped electrode device, the thin layer of dielectric results in a large capacitance which limits the device bandwidth. On the contrary, the TWGFM allows for high-speed modulation with low driving power. In our design, the Al_2O_3 thickness is chosen to be 6 nm which can be easily deposited and allows for a V_π below 5V.

III. Electrode Design

(a) Lumped Electrode

The optical structure has been designed by the above process, and we will focus on the electrical bandwidth analysis in this section. For such a fiber-based modulator with 1.372 mm-long length and a thin dielectric layer, the conventional coplanar strip (CPS) lumped electrode will theoretically have a very limited bandwidth. The bandwidth of the lumped electrode-based modulator is determined by f_3dB=1/2πRC where R and C is the total resistance and capacitance respectively. The resistance is calculated considering the graphene ohmic resistance and the contact resistance between the graphene and the electrode:

$$R_{Graphene} = \frac{\rho}{\Delta} * \frac{2*W+S}{L} \quad (2)$$

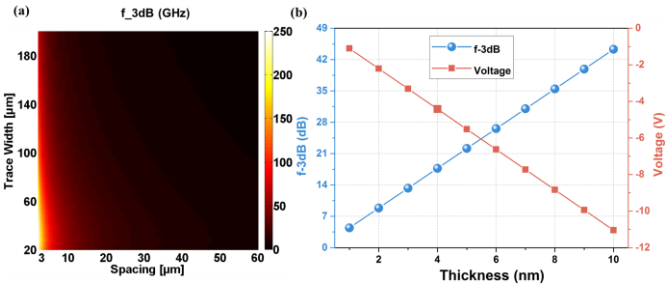

Fig.5. (a) The simulated contour map of the lumped electrode's 3dB bandwidth of under different electrode widths and spacings. (b) For an electrode width of 100 μm and spacing of 10 μm, the calculated f-3dB and the required V_π.

$$R_{Contact} = \frac{R_c}{2*W+S} \quad (3)$$

where ρ is the graphene resistivity, Δ is the graphene thickness, W is the electrode strip width, and S is the electrode gap distance. The R_c is chosen to be 400 Ω-μm as the contact resistance [27]. The capacitance is calculated by considering a parallel plate oxide capacitance in series with the top and bottom graphene quantum capacitance. The bandwidths calculated under various electrode widths and gap distances are shown in Fig. 5 (a). It can be seen that for most of the electrode designs, the electrical bandwidth is limited to less than 50 GHz. For an extreme case with two narrow metal strip lines which are very close to each other, the bandwidth can be very high as shown in the lower left corner of the figure. The predicted bandwidth can reach to >100 GHz when the gap distance is below 5 μm. But this is not practical since the narrow metal strip and electrode gap will induce optical loss, and it is very difficult to handle the microfiber. The photo mask requires higher resolution, and hence higher cost as well.

The capacitance of the lumped electrode can be greatly reduced if thicker oxide layer is used, but the required driving voltage will increase significantly. We consider an electrode with 100 μm-trace width and 10 μm-gap distance. Then we calculate the 3dB bandwidth and the required driving voltage for Fermi level tuning from 0.5 eV to 0.9 eV with different oxide thickness as shown in Fig. 5 (b). The 3-dB bandwidth can reach to nearly 50 GHz with 10 nm-thick dielectric. But as we mentioned, the required V_π increases to more than 11V which is not practical.

(b) Traveling Wave Electrode

To achieve high-speed operation, the traveling wave electrodes are designed by optimizing the EE S_{21} response

This article has been accepted for publication in a future issue of this journal, but has not been fully edited. Content may change prior to final publication. Citation information: DOI 10.1109/JLT.2018.2864606, Journal of Lightwave Technology

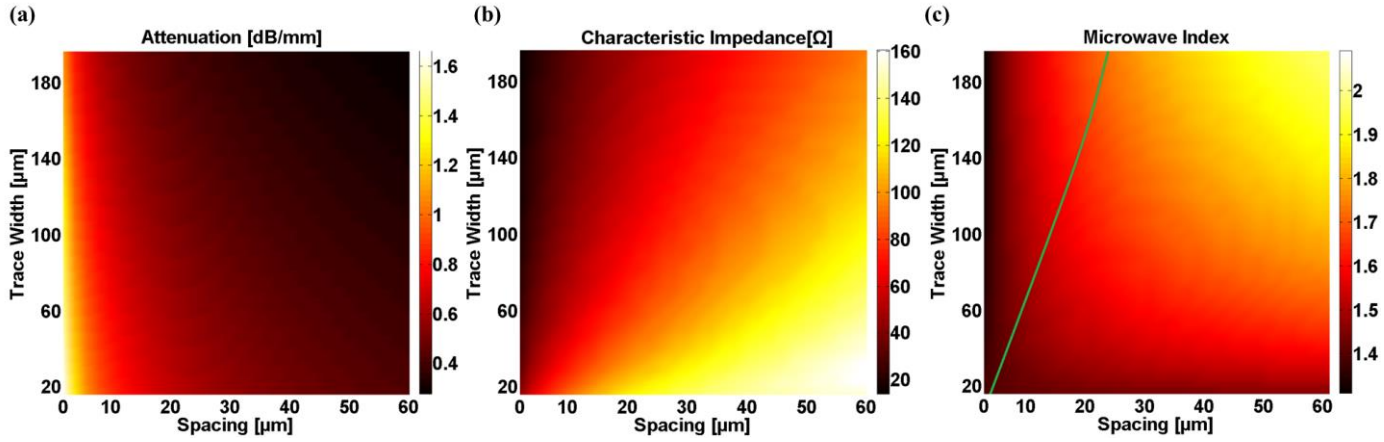

Fig.6. The simulated contour map of the: (a) microwave attenuation, (b)effective phase index, and (c) characteristic impedance under different electrode structures.

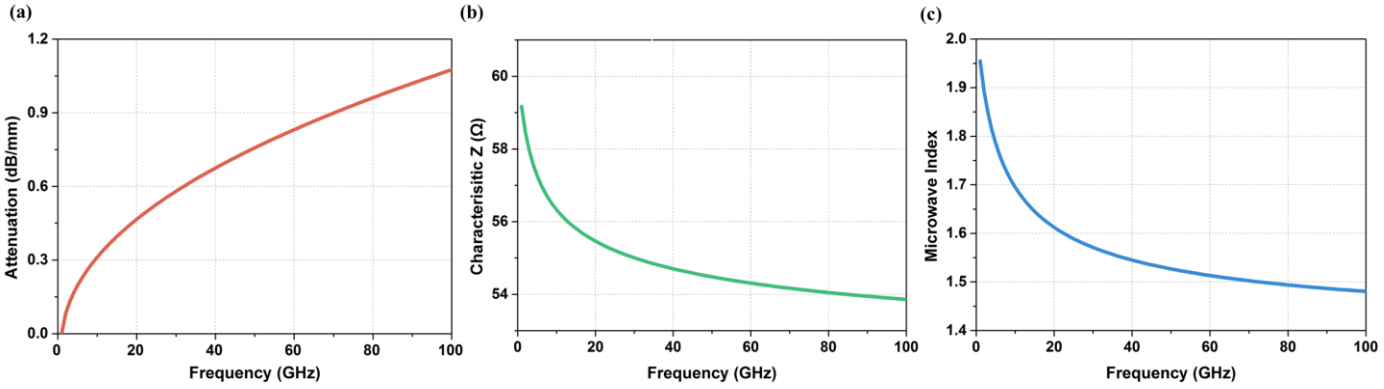

Fig.7. Simulated frequency dependent (a) microwave attenuation, (b) microwave index, and (c) characteristic impedance of CPS electrode for the electrode with 176 μm-strip width and 12 μm-gap distance.

with a 3-D full-wave electromagnetic solver. Since the optical group index is small, a CPS electrode structure can be used. There are three requirements for a high-speed TWE: a) low microwave attenuation; b) group velocity matching between the microwave and optical wave; c) impedance matching between the transmission line and the termination [28]. The electrode model is built in an electromagnetic solver, and the frequency response is numerically calculated by FEM. The modulator length has been determined to be 1.372 mm in the optical waveguide design. The electrode material is chosen to be silver, and its thickness is set to be 2 μm here. The remaining parameters that need to be optimized are the electrode width W and the electrode gap distance S. We simulate the s-parameters of different electrode structures, and the s-parameters are then converted to ABCD parameters using the method that has been previously summarized in [29]. Then, the RF attenuation α, characteristic impedance Z, and microwave effective index n, are calculated from the ABCD parameters. Since these parameters are all frequency dependent, we vary the structural parameters of the electrodes, and the α, n and Z values at different frequencies from 40 GHz to 120 GHz are obtained. It can also be seen that the characteristic impedance and the microwave index do not change too much at the frequencies higher than 80 GHz. The microwave attenuation keeps increasing as the frequency increases, but at a much lower rate. Thus, we choose the 80 GHz case to simplify the electrode design. The α, Z, and n parameters at 80 GHz as a function of the electrode width and the electrode gap distance are calculated and shown in Fig. 6 (a), (b), (c), respectively. The structural parameters should be determined by considering the requirements of low RF loss, group velocity matching and the impedance matching. The low RF attenuation can be realized by using wide metal strips with a large spacing. When the electrode spacing is larger than 30 μm, the microwave loss will not reduce too much further which is due to the dominant skin effect at high frequency. With the same electrode geometry, the metal with higher conductivity such as silver and copper can be used to reduce the RF loss. The characteristic impedance increases with larger electrode spacing and narrower trace width, as shown in Fig. 6 (b). The microwave index is simulated under different structural parameters as plotted in Fig. 6 (c). Unlike silicon modulator, the GFM has a small group index of 1.378. The group velocity of the RF signal can be simply slowed down by reduction of the electrode width or spacing. To better find the matching point, the structural parameters with 50-ohm characteristic impedance is plotted as a green curve in Fig. 6 (c). The electrode design should be determined using the values near this curve while avoiding the high RF loss as well. Another issue is the spacing between the electrodes should be at least 10 μm for low optical loss, low cost of the lithography mask and easy transfer process of the microfiber. Taking the above considerations into account, the only region that may be used is the left upper corner of Fig. 6 (c). That is large trace width (above 150 μm) and relatively narrow electrode spacing. We choose a trace width of 176 μm

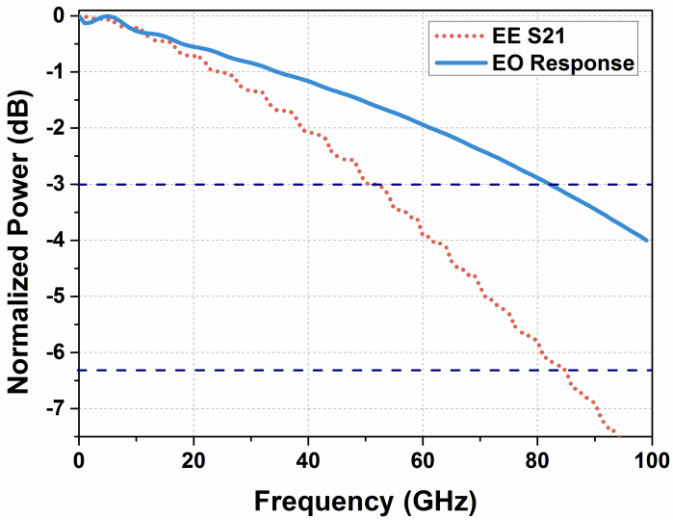

Fig.8. The simulated EE S21 response and EO frequency response (dashed lines mark -3 dB and -6.4 dB).

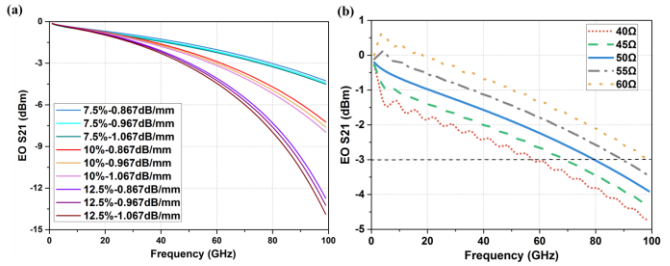

Fig.9. (a) The simulated EO frequency response under different percentages of index mismatch and different RF attenuations. (b) The simulated EO frequency response under different characteristic impedances.

and a gap distance of 12 μm. The corresponding frequency dependent RF attenuation, characteristic impedance and the microwave index are calculated and plotted in Fig. 7 (a), (b), (c), respectively. The RF loss increases at higher frequency regime and the attenuation is ~ 0.967 dB/mm at 80 GHz. We can achieve a characteristic impedance of ~ 54 ohm at this frequency which is quite close to the target of 50 ohm. It can be seen that the microwave index is a bit larger than the optical wave index, and we believe that it is the main limiting factor of the modulation bandwidth. By using such an electrode structure, we have simulated the EE and EO frequency response as shown in Fig. 8. The 3-dB EO bandwidth is ~ 82 GHz and the 6.4-dB EE bandwidth is ~ 84 GHz. This inconsistency is due to the 7.38 % index mismatch between the RF and the optical wave. If the microwave index mismatch is further reduced, the EE and EO bandwidth will become closer. We also investigate how the RF attenuation; characteristic impedance and the microwave index affect the EO performance of the modulator. We calculate the EO frequency response with different RF attenuation and index mismatch as shown by the plots in Fig. 9 (a). The EO bandwidth drops from 82 GHz to 64 GHz when the mismatch increases from 5% to 7.5%. The bandwidth will be below 50 GHz if there exists 10% index mismatch. The $\pm$0.1 dB/mm change in RF attenuation has a much less impact on the frequency response compared with the index mismatch between the optical and microwave. The EO frequency responses with different characteristic impedances are plotted in Fig. 9 (b). It can be seen that the characteristic impedance mismatch does not degrade the performance too much as well. The smaller impedance has increased bandwidth can be attributed to impedance mismatch induced reflections that results in the signal pre-emphasis [30]. The results reveal that the index matching between optical and microwave is very important for the high-speed operation. The performance will be degraded significantly if the index mismatch increases.

IV. Conclusion

To conclude, we have proposed and designed an all-in-fiber electro-optic modulation using graphene/microfiber structure. The modulator length is 1.372 mm, and the fiber diameter is 2.2 μm. A low V_π of only 4.9 V and a low optical loss of only 1.6 dB are achieved, which can be well compatible with the fiber systems. We have quantitively investigated the bandwidth limitation of the lumped electrode-based modulator. Then, a TWGFM is designed with a very high 3-dB bandwidth of 82 GHz.

Acknowledgement

The authors thank Prof. Zhenzhou Cheng for the useful discussions.

References

[1] F. Xia, T, "Ultrafast graphene photodetector," *Nature Nanotechnology*, vol. 4, pp. 839–843, Dec. 2009.

[2] X. Wang, Z. Cheng, K. Xu, H. K. Tsang, and J. B. Xu, "High-responsivity graphene/silicon-heterostructure waveguide photodetectors," *Nature Photonics*, vol. 7, no. 11, pp. 888-891, Nov., 2013.

[3] A. Pospiscil, M. Humer, M. M. Furchi, D. Bachmann, R. Guider, T. Fromherz, and T. Mueller, "CMOS-compatible graphene photodetector covering all optical communication bands," *Nature Photonics*, vol. 7, pp. 892-896, Sep., 2013.

[4] T. Gu, N. Petrone, J. F. McMillan, A. Zande, M. Yu, G. Q. Lo, D. L. Kwong, J. Hone, and C. W. Wong, "Regenerative oscillation and four-wave mixing in graphene optoelectronics," *Nature Photonics*, vol. 6, pp. 554-559, Jul., 2012.

[5] Y. Wu, B. Yao, Y. Cheng, Y. Rao, Y. Gong, X. Zhou, B. Wu, and K. S. Chiang, "Four-wave mixing in a microfiber attached onto a graphene film," *IEEE Photon. Technol. Lett.*, vol. 26, no. 3, pp. 249-252, Feb., 2014.

[6] Y. H. Lin and G. R. Lin, "Kelly sideband variation and self four-wave-mixing in femtosecond fiber soliton laser mode-locked by multiple exfoliated graphite nano-particles," *Laser Phy. Lett.*, vol. 10, no. 4, Mar, 2013.

[7] W. J. Cao, H. Y. Wang, A. P. Luo, Z. C. Luo, and W. C. Xu, "Graphene-based, 50 nm wide-band tunable passively Q-switched fiber laser," in *Laser Phy. Lett.*, vol. 9, no. 1, pp. 54, Nov., 2011.

[8] G. Sobon, J. Sotor, I. Pasternak, K. Grodecki, P. Paletko, W. Strupinski, Z. Jankiewicz, and K. M. Abramski, "Er-doped fiber laser mode-locked by CVD-graphene saturable absorber," *J. Ligtw. Technol.*, vol. 30, no. 17, pp. 2770-2775, Sep., 2012.

[9] Z. T. Wang, Y. Chen, C. J. Zhao, H. Zhang, S. C. Wen, "Switchable dual-wavelength synchronously Q-switched erbium-doped fiber laser based on graphene saturable absorber," *IEEE Photon. Journal*, vol. 4, no. 3, pp. 869-876, Jun., 2012.

[10] Q. Bao, H. Zhang, B. Wang, Z. Ni, C. Haley, Y. Lim, Y. Wang, D. Tang, and K. P. Loh, "Broadband graphene polarizer," *Nature Photonics*, vol. 5, pp. 411-415, May, 2011.

[11] M. Liu, X. Yin, E. U. Avila, B. Geng, T. Zentgraf, L. Ju, F. Wang, and X. Zhang, "A graphene-based broadband optical modulator," *Nature*, vol. 474, no. 2, pp. 64-67, Jun, 2011.

[12] K. Xu, L. Yang, J. Sung, Y. Chen, Z. Cheng, C. W. Chow, C.-H. Yeh, and H. K. Tsang, "Compatibility of Silicon Mach-Zehnder Modulators for Advanced Modulation Formats," *J. Lightw. Technol.*, vol. 31, no. 15, pp. 2550 - 2554, Aug. 2013.

[13] K. Xu, C. Y. Wong, L. Zhang, L. Liu, N. Liu, C. W. Chow, and H. K. Tsang, "56 Gbit/s DMT signal generated by an integrated silicon ring modulator," *in CLEO*, San Jose, Stu1G.7, 2016.

[14] W. Li, B. Chen, C. Meng, W. Fang, Y. Xiao, X. Li, Z. Hu, Y. Xu, L. Tong, H. Wang, W. Liu, J. Bao, and Y. Shen, "Ultrafast all-optical graphene modulator," *Nano. Lett.*, vol. 14, no. 2, pp. 955-959, Jan., 2014.

[15] J. Chen, B. Zheng, G. Shao, S. Ge, F. Xu, and Y. Q. Lu, "An all-optical modulator based on a stereo graphene–microfiber structure," *Light: Science and Applications*, vol. 4, Dec., 2015.

[16] S. Yu, X. Wu, K. Chen, B. Chen, X. Guo, D. Dai, L. Tong, W. Liu, and Y. Shen, "All-optical graphene modulator based on optical Kerr phase shift," *Optica*, vol. 3, no. 5, pp. 541-544, May, 2016.

[17] Z. Liu, M. Feng, W. Jiang, W. Xin, P. Wang, Q. Sheng, Y. Liu, D. Wang, W. Zhou, and J. Tian, "Broadband all-optical modulation using a graphene-covered-microfiber," *Laser Phy. Lett.*, vol. 10, no. 6, Feb., 2013.

[18] M. Liu, X. Yin, and X. Zhang, "Double-layer graphene optical modulator," *Nano. Lett.*, vol. 12, no. 3, pp. 1482-1485, Feb., 2012.

[19] C. Xu, Y. Jin, L. Yang, J. Yang, and X. Jiang, "Characteristics of electro-refractive modulating based on graphene-oxide-silicon waveguide," *Opt. Express*, vol. 20, no. 20, pp. 22398-22405, Sep., 2012.

[20] Y. Hu, M. Pantouvaki, J. V. Campenhout, S. Brems, I. Asselberghs, C. Huyghebaert, P. Absil, D. V. Thourhout, "Broadband 10 Gb/s operation of graphene electro-absorption modulator on silicon," *Laser & Photonics Review*, vol. 10, no. 2, pp. 307-316, Mar., 2016.

[21] T. Xiao, Z. Cheng, and K. Goda, "Graphene-on-silicon hybrid plasmonic-photonic integrated circuits," *Nanotechnology*, vol. 28, no. 24, pp. 245201, May, 2017.

[22] C. T. Thare, Y. H. Daniel Lee, J. Cardenas, and M. Lipson, "Graphene electro-optic modulator with 30 GHz bandwidth," *Nature Photonics*, vol. 9, pp. 511-514, Jul, 2015.

[23] M. Fan, H. Yang, P. Zheng, G. Hu, B. Yun, and Y. Cui, "Multilayer graphene electro-absorption optical modulator based on double-stripe silicon nitride waveguide," *Opt. Express*, vol. 25, no. 18, pp. 21619-21629, Sep., 2017.

[24] Q. Bao and K. P. Loh, "Graphene Photonics, Plasmonics, and Broadband Optoelectronic Devices," *ACS Nano*, vol. 6, no. 5, pp. 3677-3694, Apr., 2012.

[25] A. Felipe, G. Espindola, H. J. Kalinowski, J. A. S. Lima, and A. S. Paterno, "Stepwise fabrication of arbitrary fiber optic tapers," *Opt. Express*, vol. 20, no. 18, pp. 19893-19904, Aug., 2012.

[26] A. Phatak, Z. Cheng, C. Qin, and K. Goda, "Design of electro-optic modulators based on graphene-on-silicon slot waveguides," *Opt. Lett.*, vol. 41, no. 11, pp. 2501-2504, Jun., 2016.

[27] S. J. Koester and M. Li, "High-speed waveguide-coupled graphene-on-graphene optical modulators," *Applied Phy. Lett.*, vol. 100, no. 17, pp. 171107, Apr., 2012.

[28] Z. Han, S. Tang, D. An, L. Sun, X. Lu, Z. Shi, Q. Zhou, and R. T. Chen, "High-speed travelling-wave electrodes for polymeric electro-optic modulators," in *SPIE Conf. Optoelectronic Interconnects VI*, San Jose, CA, vol. 3632, 1999.

[29] D. A. Frickey, "Conversions between S, Z, Y, h, ABCD, and T parameters which are valid for complex source and load impedances," *IEEE Trans. Microwave Theory and Techniques*, vol. 42, no. 2, pp. 205-211, Feb., 1994.

[30] H. Yu, and W. Bogaerts. "An Equivalent Circuit Model of the Traveling Wave Electrode for Carrier-Depletion-Based Silicon Optical Modulators." *Journal of Lightwave Technology*. vol. 30, no. 11, pp. 1602-1609, June, 2012.